DOE/SC-ARM-TR-307

Plan Position Indicator Hydrometeor Field Statistics (PPIHYD) Evaluation Data Product Version 1.0

I Silber JM Comstock

August 2024

DOE/SC-ARM-TR-307

Plan Position Indicator Hydrometeor Field Statistics (PPIHYD) Evaluation Data Product Version 1.0

I Silber
JM Comstock
Both at Pacific Northwest National Laboratory

August 2024

How to cite this document:

Silber, I, and JM Comstock. Plan Position Indicatory Hydrometeor Field Statistics (PPIHYD) Evaluation Data Product Version 1.0. 2024. U.S. Department of Energy, Atmospheric Radiation Measurement user facility, Richland, Washington. DOE/SC-ARM-TR-307.

Work supported by the U.S. Department of Energy,
Office of Science, Office of Biological and Environmental Research

Executive Summary

The PPIHYD evaluation data product provides distinct hydrometeor field statistics calculated from U.S. Department of Energy Atmospheric Radiation Measurement (ARM) user facility scanning radar plan position indicator (PPI) scans. These statistics include the equivalent reflectivity factor and Doppler spectral width percentiles, min/max values, and first four moments (mean, standard deviation, skewness, and kurtosis) of distinct hydrometeor features (clustered hydrometeor fields). Statistics also include morphological properties, water content and precipitation rate parameterization-based estimates, and thermodynamic properties interpolated using the Interpolated Sonde value-added product (INTERPSONDE VAP). The data set is organized in tabular form and is accompanied by mask arrays with corresponding indices. This straightforward file structure simplifies scanning radar data processing and renders this data set useful for process understanding and model evaluation studies. This report describes the data set and its processing algorithm and provides some examples.

Acronyms and Abbreviations

ARM	Atmospheric Radiation Measurement
COMBLE	Cold-Air Outbreaks in the Marine Boundary Layer Experiment
FOV	field of view
INTERPSONDE	Interpolated Sonde
KASACR	Ka-Band Scanning ARM Cloud Radar
KAZR	Ka-Band ARM Zenith Radar
netCDF	Network Common Data Form
PPI	plan position indicator
PPIHYD	Plan Position Indicator Hydrometeor Field Statistics
Py-ART	Python ARM Radar Toolkit
QC	quality control
RoI	radius of influence
SACR	Scanning ARM Cloud Radar
SNR	signal-to-noise ratio
TRACER	Tracking Aerosol Convection Interactions Experiment
UTC	Coordinated Universal Time
VAP	value-added product

Contents

Figures

1.0 Introduction

Clouds and precipitation processes impact the water cycle and the surface and atmospheric energy budgets from low to high latitudes. Because of these and other cloud effects, there is interest in understanding, characterizing, and properly representing cloud states and processes in models. However, in each of these aspects, there are still significant deficiencies (e.g., Feingold et al. 2022, Kay et al. 2018, McCoy et al. 2015).

On a large scale, cloud microphysical structure and macrophysical morphology determine the magnitude of cloud radiative effects. Cloud spatial morphology can be robustly characterized by space-borne instruments onboard geostationary satellites at a high temporal resolution at lower latitudes and using occasional overpasses of polar-orbiting satellites at higher latitudes. However, due to the dominating radiative footprint of the cloud top region, cloud microphysical properties and precipitation fields below the cloud top are highly uncertain and challenging to characterize. Because the spatial variability of these quantities is considered within the sub-grid scale of the vast majority of large-scale models, sub-grid-scale parameterizations can have a crucial influence on model simulations. Therefore, expanding the observational database of clouds and precipitation "sub-grid-scale" spatial variability is essential to evaluate existing parameterizations and provide a basis for new parameterizations (e.g., Covert et al. 2022, Song et al. 2018).

ARM scanning radars, though relatively limited in range and spatial coverage, provide unique information about the spatial variability of cloud and precipitation field microphysics. They can inform about precipitation rates, water content, wind component variability, hydrometeor shape, and more. These data sets can, generally speaking, be used to directly evaluate models and their implemented sub-grid-scale assumptions, either by comparing retrieved with simulated quantities or by using instrument simulators (e.g., Silber et al. 2022) to evaluate simulated radar observables directly. Nevertheless, with the typically non-trivial use and processing of scanning radar data sets, these valuable data sets often remain under used, even with the availability of powerful and free tools such as the Python ARM Radar Toolkit (Py-ART; Helmus and Collis 2016). Here, we describe the Plan Position Indicator Hydrometeor Field Statistics (PPIHYD) data set, which makes information extracted from scanning radar PPI data more accessible and easier to use. PPIHYD includes spatial statistics based on distinct hydrometeor features (clustered hydrometeor fields) and leverages the information derived from scanning radar measurements. It is based on ARM scanning radar PPI scans and currently provides information about the spatial variability of radar moment, estimates of water contents, and precipitation rates per detected feature.

2.0 Algorithm and Methodology

The PPIHYD processing algorithm is described by the flowchart in Figure 1. Processing procedures leverage algorithms from multiple Python packages, including Py-ART, tobac (Heikenfeld et al. 2019), and scikit-image (van der Walt et al. 2014).

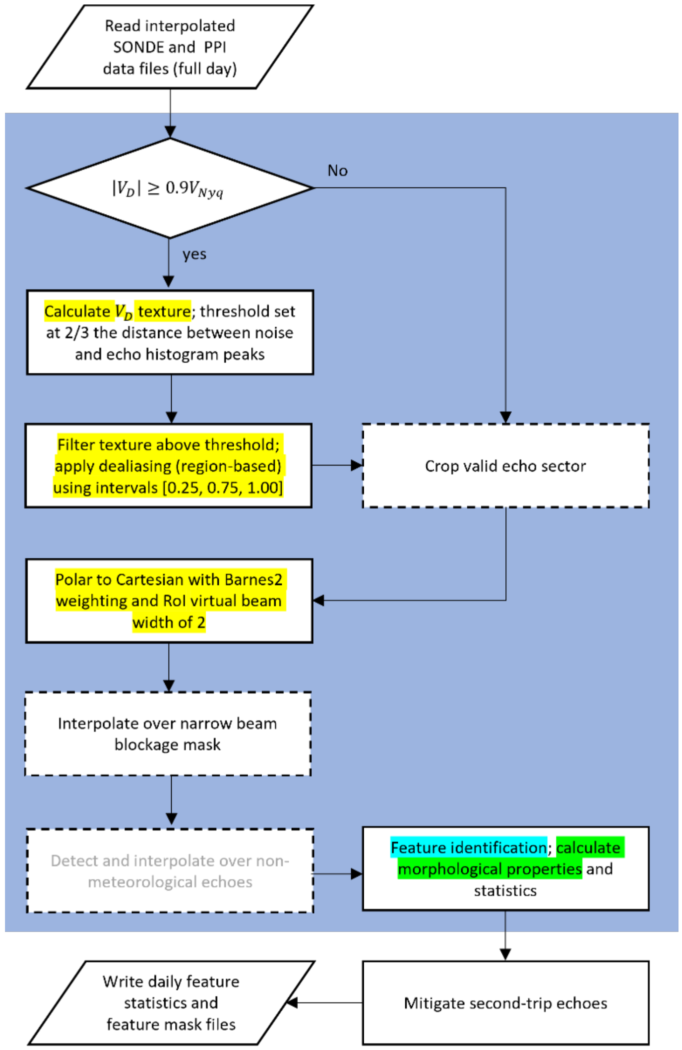

Figure 1. Flowchart of PPIHYD processing algorithm. V_D and V_{Nyq} denote the mean Doppler and Nyquist velocities, respectively. Yellow, cyan, and green highlighted text denotes processes using Py-ART, tobac, and scikit-image algorithms. The grey font color indicates planned code development. The steps in the foreground of the shaded rectangle are applied separately on sweeps.

PPIHYD is designed to be applied to quality controlled (QCed) and partially corrected PPI scan files (b1 or c1 datastreams). (Because some of the processing steps are performed prior to Cartesian gridding, gridded ARM data sets are not used in PPIHYD's processing.) After files covering a full given day are loaded, PPI radar sweeps are processed separately. Observed hydrometeor field properties are more likely to change significantly at high-elevation angle scans (e.g., when crossing the melting level), especially in large hydrometeor fields extending over large radial distances. Therefore, the PPIHYD processing and output data files are limited to sweeps at low-elevation angles of up to a few degrees, supporting more straightforward analysis and evaluation of, mostly precipitating, hydrometeor fields. PPI scans persistently suffering from ground-clutter effects (e.g., some 0° elevation configurations) are excluded from PPIHYD processing. The different processing steps depicted in Figure 1 are discussed below.

2.1 Doppler Velocity Dealising

A Py-ART region-based dealiasing procedure is first performed for suspected folding indicated by the mean Doppler velocity (V_D) exceeding an arbitrary fraction of 0.9 of the Nyquist velocity (N_{Nyq}) in at least one sampled voxel in the sweep. Before calling the dealiasing algorithm, the V_D field texture is calculated, and values exceeding an automatically determined threshold value are filtered out. Because dealiasing procedures are complex and often require manual tweaking, whereas here, dealiasing is applied automatically, we flag all dealiased sweeps and, in general, only report a single field that is based on V_D data (the V_D standard deviation per feature). Because it is based on a radial wind component, this output field should be used with caution, especially in dealiased sweeps.

2.2 Exclusion of Extensive Beam Blockage Sectors

Because the robustness of detected features requires spatial continuity, persistent beam blockage could bias feature determination and statistics. Beam blockage treatment is separated here to the removal of narrow beam blockage as a result of nearby obstructions (buildings, antenna towers, etc.), which are processed after Cartesian gridding (Section 2.4) and extended blockage by terrain. The effects of extended beam blockage are removed by excluding entire scan sectors from processing, ideally close to scan azimuth range limits, after manual characterization of elevation-dependent, blockage-free sectors in the radar field of view (FOV). Removal of scan sectors influenced by extended beam blockage is demonstrated in Figure 2 using Ka-Band Scanning ARM Cloud Radar (KASACR) PPI measurements at 0.5° elevation from the Cold-Air Outbreaks in the Marine Boundary Layer Experiment (COMBLE; Geerts et al. 2022). Given the fixed nature of obstacles generating these blockage artifacts, removal sectors should require elevation-dependent characterization only once per deployment (unless a scanning radar is repositioned during a deployment or changes its scan strategy).

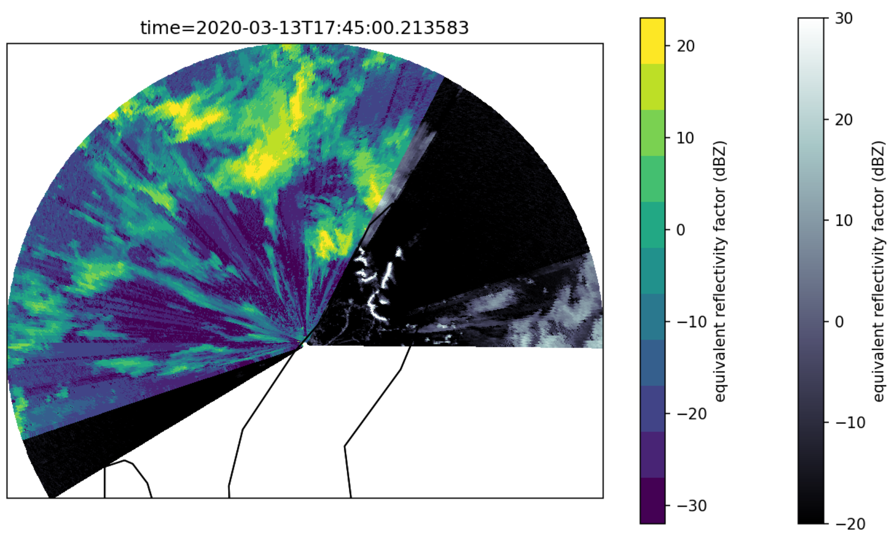

Figure 2. Removal of scan sectors extensively affected by beam blockage (greyscale sectors), demonstrated on a KASACR 0.5° elevation PPI scan from COMBLE on March 13, 2020 at 17:45 UTC.

2.3 Data Set Gridding

At this point, each radar sweep is gridded from a polar to a Cartesian coordinate system. Here, we use Py-ART's gridding method. The radius of influence (RoI) determining all radar samples relevant for a Cartesian grid cell based on their distance from the grid cell, is calculated using a virtual beam width of 2°, while ignoring the vertical (z) dimension, i.e., considering only horizontal distances. Samples within the RoI are then weighted using a modified Barnes weighting function (Barnes 1964, Pauley and Wu 1990). This type of weighting results in minimal data smoothing, which is helpful in removing sparse noise.

2.4 Narrow Beam Blockage Mitigation

The lack of certain fields in Scanning ARM Cloud Radar (SACR) measurements, such as the normalized coherent power, for example, renders data artifact removal a challenging task. Among some of the challenges is the treatment of narrow scan sectors influenced by nearby obstacles. Such narrow beam blockage artifacts can be characterized once per deployment because they are also fixed, similar to extensive beam blockage sectors. However, because multiple artifacts per elevation angle could potentially result in feature discontinuity, impacting the data set's value, narrow beam blockage is followed by interpolating the affected data.

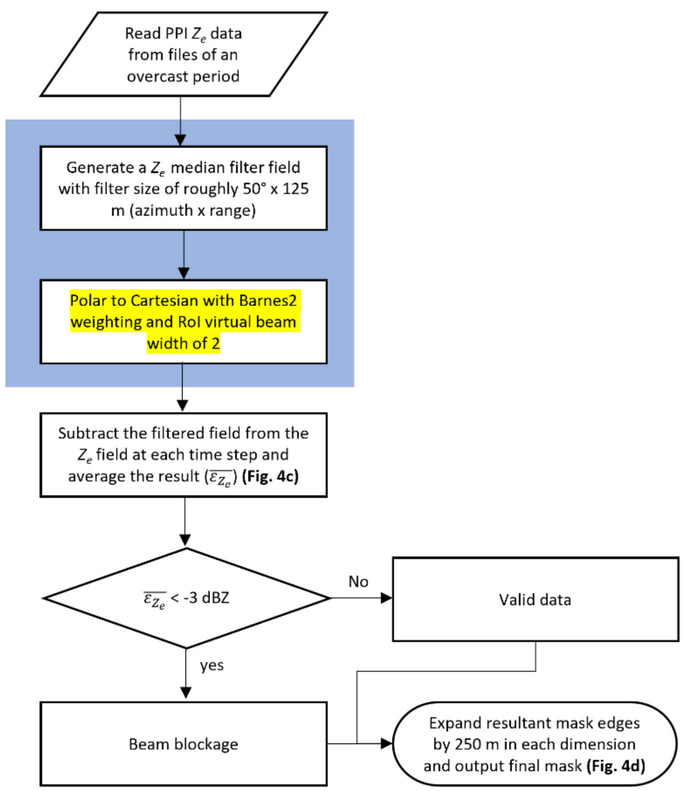

Figure 3. Flowchart of narrow beam blockage detection algorithm. Z_e denotes the equivalent reflectivity factor, and $\boldsymbol{\varepsilon_{Z_e}}$ the temporally averaged median filtered Z_e deviation from the non-filtered Z_e. Yellow highlighted text denotes processes using Py-ART algorithms. The steps in the foreground of the shaded rectangle are applied separately on sweeps.

The identification of narrow beam blockage is still experimental, but preliminary results using data from the Tracking Aerosol Convection Interactions Experiment (TRACER; Jensen et al. 2023) show satisfactory results. A self-explanatory flowchart describing the narrow beam blockage detection algorithm is shown in Figure 3.

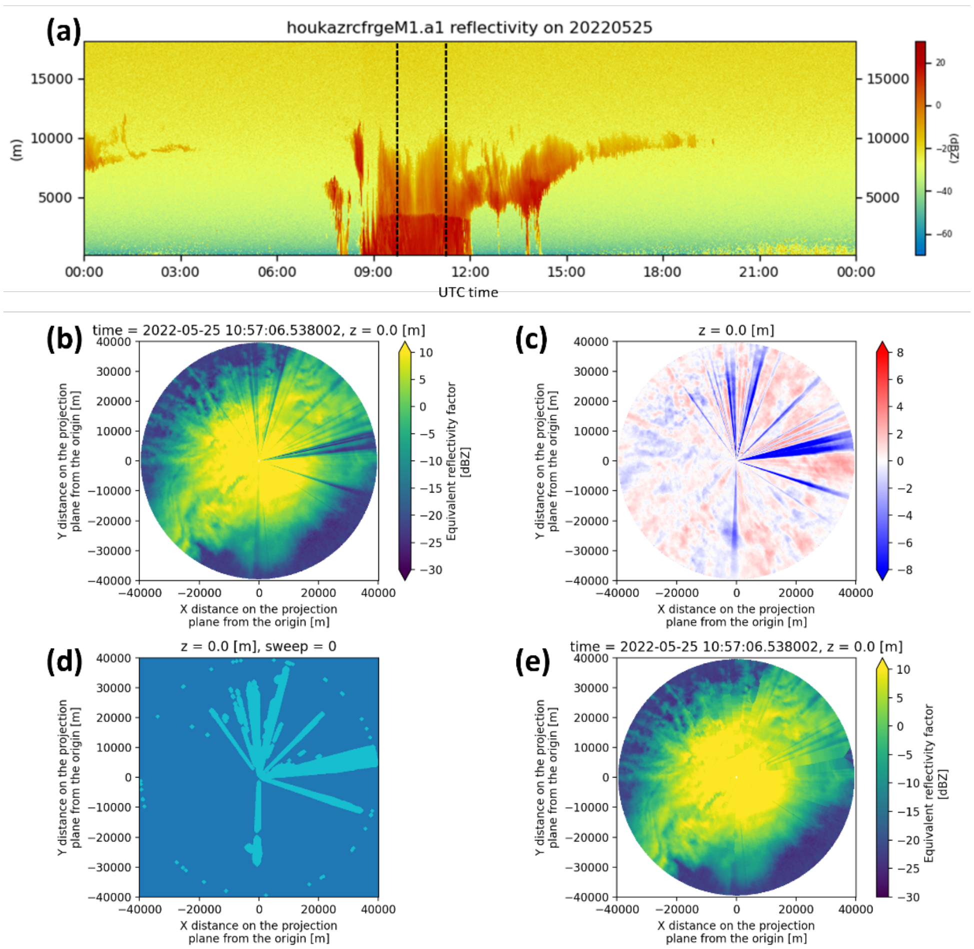

Figure 4. Beam blockage detection example for TRACER KASACR PPI scans at 1.0° elevation. (a) Height-time curtain plot of Ka-Band ARM Zenith Radar (KAZR; (Widener et al. 2012) equivalent reflectivity factor (Z_e) from February 25, 2022, taken from the ARM DQ Plot Browser. The vertical dashed lines designate the period from which 10 consecutive PPI scan files were used for processing. (b) KASACR PPI sweep at 10:57 UTC. (c) Time-average of median filtered Z_e deviation from the non-filtered Z_e. (d) The resultant narrow beam blockage mask (brighter regions), which can be applied to TRACER PPI scans at a 1.0° elevation. (e) Z_e field from the 10:57 UTC PPI sweep with beam-blockage regions interpolated using the nearest-neighbor method.

Figure 4 demonstrates the narrow beam blockage mask determination and interpolation using TRACER KASACR PPI scans at 1.0° elevation. After an overcast period is found (Figure 4a), equivalent reflectivity factor (Z_e) field data from PPI scans during that period are loaded and gridded onto a Cartesian grid (Figure 4b depicts a single sweep). By evaluating the time-averaged deviation of the Z_e field from its median-filtered value (Figure 4c), one can extract the beam blockage mask. The final mask is received following an artificial mask expansion to consider voxels that are only partially influenced by the beam blockage (Figure 4d). This final mask can be applied to all TRACER KASACR sweeps at the examined elevation angle. As a final step, all voxels influenced by the beam blockage are filled using a nearest-neighbor interpolation, as shown in Figure 4e. This interpolation is required to prevent artificial hydrometeor feature separation. Interpolated values are excluded from statistics calculations (Section 2.6), except for the morphological analysis, in which their impact is generally minor. Hydrometeor features in which the artificially filled fraction of voxels (which will include an insect-detection mask at a later stage of development – Section 2.5) exceeds 0.10 are flagged.

2.5 Removal of Non-Meteorological Echoes

A processing step of detecting and interpolating over non-meteorological echoes (insects, birds, etc.) is suggested from Figure 1. This processing step requires dedicated analysis and code development planned for future PPIHYD versions. Note that while this step's flowchart position suggests post-gridding processing, the implemented methodology might eventually be generalized, such that it will take place prior to gridding. Such an implementation in polar coordinates will enable its application to other, lower-level, scanning radar datastreams.

2.6 Feature Identification and Statistics Calculations

Hydrometeor field features are identified (clustered) by leveraging the tobac package's feature detection and segmentation methods (see Heikenfeld et al. 2019). Current PPIHYD processing does not include feature tracking, owing to its reduced value given the commonly used relatively short maximum range of ARM SACRs and the low repetition frequency of ARM radar PPI scans. However, the tobac output required for straightforward tracking applications is retained in PPIHYD's output files, should it be useful for users.

The identification process is applied to the Z_e field using three deployment-dependent thresholds differentiated by 0.5 dBZ increments. These threshold sets are determined based on expert judgment after inspection of the data, and differ between deployments because of the differences in operated instruments and scan strategies, reflected in different Z_e sensitivities. Applying such thresholds can occasionally mitigate the influence of some faint second-trip echoes, as demonstrated when the Z_e field depicted in Figure 2 is compared to the same field plotted in the right panel of Figure 5 while highlighting values above the COMBLE Z_e threshold set of -12.5, -12.0, and -11.5 dBZ. We note that PPIHYD uses Z_e for this processing rather than other fields, such as signal-to-noise ratio (SNR), because Z_e thresholds ostensibly provide more straightforward data interpretation and model output evaluation.

Following feature identification, feature morphological properties and statistics are calculated (Section 4.0). Morphological properties are determined using the scikit-image Python package. Some thermodynamic properties are derived from vertically interpolated INTERPSONDE (Fairless et al. 2021) data fields.

2.7 Second-Trip Echo Mitigation

PPIHYD currently employs a second-trip echo mitigation routine, which leverages the morphological properties calculated for each detected feature in the previous step. Specifically, using arbitrarily selected thresholds, the second-trip mitigation routine examines ellipse fits' orientation angles and aspect ratios. If, for a given feature, the orientation angle deviates by less than 15° from the angle of the ellipse fit centroid relative to the radar location (origin in the Cartesian grid), and the ellipse fit aspect ratio is smaller than 0.3, that feature is flagged as second-trip 'suspect.' If the same conditions apply but to a stricter threshold set of 7.5° and 0.15, respectively, the given feature is flagged as a second-trip 'likely'. Figure 5 demonstrates the second-trip detection routine output mask for a COMBLE KASACR PPI scan at 0.5° elevation on March 13, 2020, at 17:45 UTC. The features flagged as 'second-trip likely' illustrated in the figure are removed from the final data set.

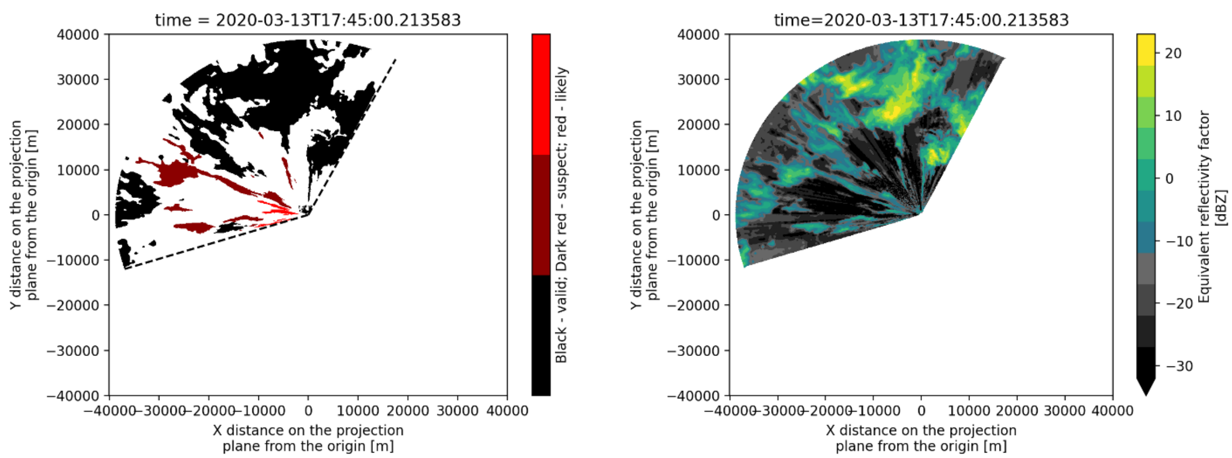

Figure 5. (Left) Second-trip detection routine output example for COMBLE KASACR PPI scans at 0.5° elevation March 13, 2020 at 17:45 UTC. Dashed lines designate the valid scan sector. Black, dark red, and red features denote valid, second-trip suspect, and second-trip likely radar echoes. Second-trip likely features are removed from the PPIHYD output. (Right) Z_e data for the same sweep illustrated here for reference. Grayscale areas designate Z_e values smaller than the $\mathbf{-12.0}$ dBZ center threshold applied in the feature detection routine (Section 2.6).

As indicated from Figure 5, some second-trip echoes directly connected to valid hydrometeor echoes are not flagged. Detection of such echoes and their detachment from valid ones requires a detailed analysis of available data fields. Similar to the planned, non-meteorological, echo detection methods, a robust method capable of detecting such common events using radar measurements, applicable to other, lower-level, scanning radar datastreams, might be developed in a polar coordinate system for future PPIHYD versions.

3.0 Input Data

The primary inputs for PPIHYD are radar moment data from scanning radar (preferentially, SACR) PPI scans. INTERPSONDE fields are used to estimate thermodynamic state variables of hydrometeor features.

4.0 Output Data

PPIHYD produces two daily output files: feature statistics and a feature mask.

The names of the output files are:

`SSS*INST*ppihydfeatXX.c1.YYYYMMDD.hhmmss.nc`

and

`SSS*INST*ppihydmaskXX.c1.YYYYMMDD.hhmmss.nc`

Where:

- `SSS` is the site
- `*INST*` is the instrument (kasacr, xsacr, wsacr, xsapr, or csapr)
- `XX` is the facility
- `YYYY` is the year
- `MM` is the month
- `DD` is the day
- `hh` is the hour
- `mm` is the minute
- `ss` is the second.

Each feature mask data file includes a numbered (indexed) mask field as its primary output. The one-dimensional (tabular) feature statistics files include numerous per-cluster variables with an index corresponding to the feature mask field. The output variables of these files include the per-feature:

- 1st, 10th, 25th, 50th, 75th, 90th, and 99th percentiles of per-feature Z_e and Doppler spectral width fields (`DMOM_pPP`, where `DMOM` is `Ze` or `sigma_D`, respectively, and `PP` is the percentile).

- Minimum (`DMOM_min`) and maximum (`DMOM_max`) values of per-feature Z_e and Doppler spectral width fields.

- First four moments of per-feature Z_e and Doppler spectral width fields (`DMOM_FMOM`, where `FMOM` is `mean`, `std`, `skewness`, or `kurtosis` referring to the mean, standard deviation, skewness, or kurtosis, respectively). Note that the moments, mostly the higher ones, are influenced by the truncated Z_e data resulting from the thresholds applied in the feature identification routine (Section 2.6).

- Number of Z_e peaks per feature with a prominence of 2, 5, and 10 times their (linear scale) surroundings (`xNN_prom_peaks`, where `NN` is 2, 5, or 10, respectively).

- Mean, minimum, and maximum values of interpolated sounding fields (temperature, relative humidity, and pressure) vertically interpolated onto the identified features (`SND_STAT`, where `SND` is `T`, `RH`, or `p`, respectively, and `STAT` is `mean`, `min`, or `max`, respectively).

- Morphological properties of detected features: area (`area`), maximum dimension (using maximum Feret diameter; `maximum_dimension`), solidity (`Solidity`), fill percent (`Fill_percent`), and ellipse fit parameters such as centroid coordinates (`ellipse_fit_centroid_x` and `ellipse_fit_centroid_y`), orientation angle from the E/W plane (`ellipse_fit_orientation`), and semi-axis lengths (`ellipse_fit_a_axis` and `ellipse_fit_c_axis`).

- Mean, standard deviation, and 99th percentile of warm rain and ice precipitation rates and ice water content estimates based on several parameterizations from the literature (`PR_REF_STAT`, where `PR` is `RR`, `SR`, and `IWC`, respectively, `REF` is the reference parameterization paper, and `STAT` is `mean`, `std`, or `p99`, respectively).

Note that the parameterization-based estimates are calculated for all detected features, regardless of parameters such as the temperature suggested by the INTERPSONDE VAP, because of long sounding release intervals and frequently occurring horizontal heterogeneity of thermodynamic fields within ARM scanning radar FOVs. Therefore, the selection of which parameterizations to use for a given scenario is left for the user to decide.

In addition to these and other per-feature variables, useful QC flags are reported as well. These QC flags include a dealiasing flag (V_D_dealiased) indicating that a dealiasing routine was applied (see Section 2.1), radar FOV edge flag (edge_flag) for hydrometeor fields extending beyond the radar FOV, large artifact fraction (artifact_frac_flag) for hydrometeor fields with a significant fraction of artifact (see Section 2.4), and a second-trip flag (second_trip_flag) denoting second-trip echo suspect (see Section 2.7).

Complete lists of output variables are given in the sample netCDF headers in Appendix A and Appendix B.

5.0 Example Plots

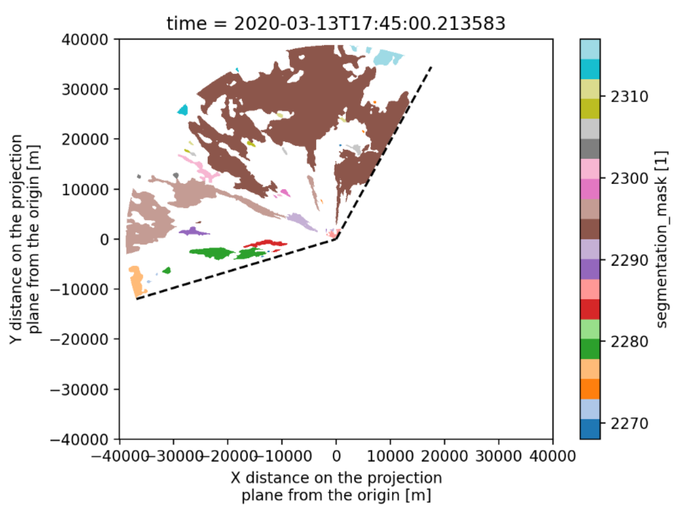

Figure 6. Feature mask (identified features) for the COMBLE KASACR PPI scan at 0.5° elevation on March 13, 2020 at 17:45 UTC.

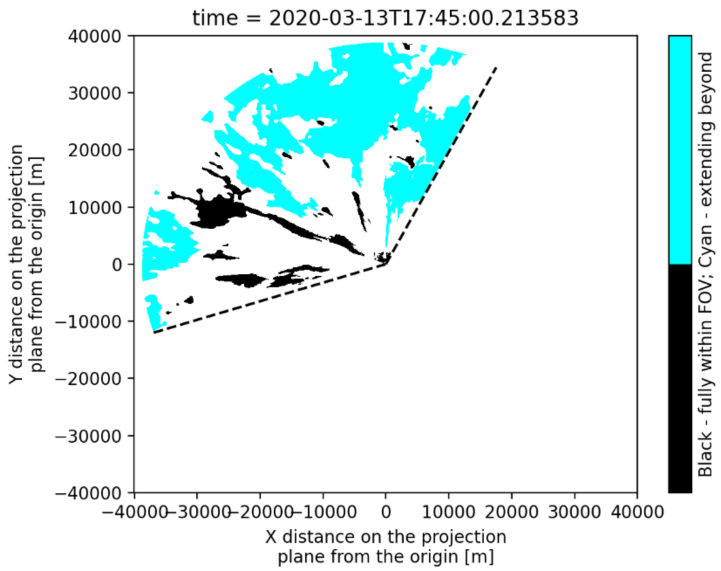

Figure 7. The feature field of view edge flag (edge_flag) projected onto the feature mask for the COMBLE KASACR PPI scan at 0.5° elevation on March 13, 2020, at 17:45 UTC.

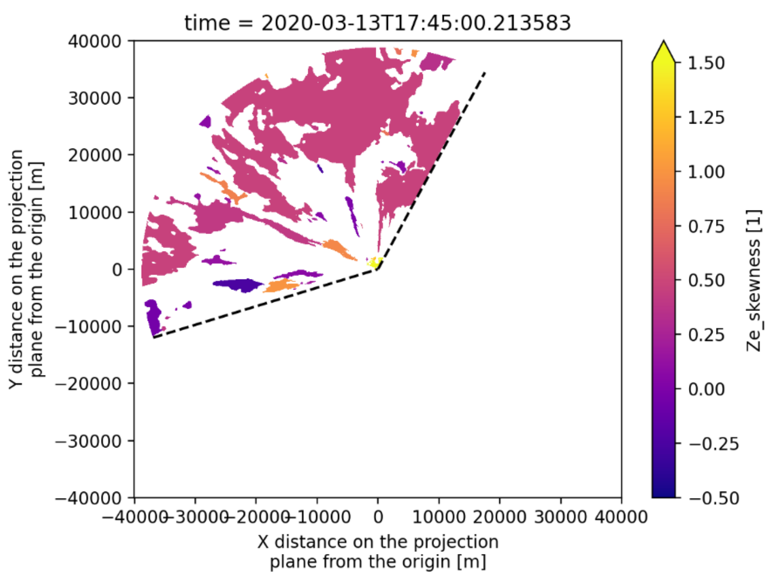

Figure 8. Feature Z_e field skewness projected onto the feature mask for the COMBLE KASACR PPI scan at 0.5° elevation on March 13, 2020, at 17:45 UTC.

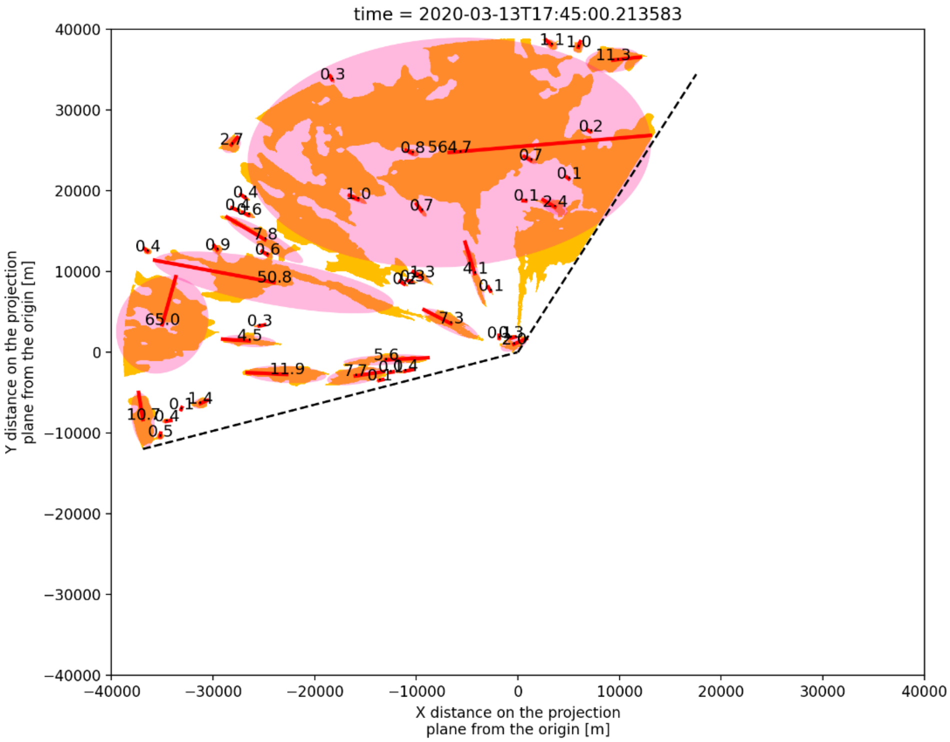

Figure 9. Morphological feature properties for the COMBLE KASACR PPI scan at 0.5° elevation on March 13, 2020, at 17:45 UTC: area in km² (numbers on feature centers), fitted ellipses (transparent pink shapes), and semi-major axes of fitted ellipses (red lines).

6.0 References

Barnes, SL. 1964. “A Technique for Maximizing Details in Numerical Weather Map Analysis.” *Journal of Applied Meteorology and Climatology* 3(4): 396–409, https://doi.org/10.1175/1520-0450(1964)003<0396:ATFMDI>2.0.CO;2

Covert, JA, DB Mechem, and Z Zhang. 2022. “Subgrid-Scale Horizontal and Vertical Variation of Cloud Water in Stratocumulus Clouds: A Case Study Based on LES and Comparisons with in situ Observations.” *Atmospheric Chemistry and Physics* 22(2): 1159–1174, https://doi.org/10.5194/acp-22-1159-2022

Feingold, G., T Goren, and T Yamaguchi. 2022. “Quantifying Albedo Susceptibility Biases in Shallow Clouds.” *Atmospheric Chemistry and Physics* 22(5): 3303–3319, https://doi.org/10.5194/acp-22-3303-2022

Geerts, B, SE Giangrande, GM McFarquhar, L Xue, SJ Abel, JM Comstock, S Crewell, PJ DeMott, K Ebell, P Field, TCJ Hill, A Hunzinger, MP Jensen, KL Johnson, TW Juliano, P Kollias, B Kosovic, C Lackner, E Luke, C Lüpkes, AA Matthews, R Neggers, M Ovchinnikov, H Powers, MD Shupe, T Spengler, BE Swanson, M Tjernström, AK Theisen, NA Wales, Y Wang, M Wendisch, and P Wu. 2022. "The COMBLE Campaign: A Study of Marine Boundary Layer Clouds in Arctic Cold-Air Outbreaks." *Bulletin of the American Meteorological Society* 103(5): E1371–E1389, https://doi.org/10.1175/BAMS-D-21-0044.1

Heikenfeld, M, PJ Marinescu, M Christensen, D Watson-Parris, F Senf, SC van den Heever, and P Stier. 2019. "Tobac 1.2: Towards a Flexible Framework for Tracking and Analysis of Clouds in Diverse Datasets." *Geoscientific Model Development* 12(11): 4551–4570, https://doi.org/10.5194/gmd-12-4551-2019

Helmus, J, and SM Collis. 2016. "The Python ARM Radar Toolkit (Py-ART), a Library for Working with Weather Radar Data in the Python Programming Language." *Journal of Open Research Software* 4(1): e25, https://doi.org/10.5334/jors.119

Fairless, T, M Jensen, A Zhou, and SE Giandrande. 2021. Interpolated Sonde and Gridded Sonde Value-Added Products. Atmospheric Radiation Measurement user facility, Richland, Washington. DOE/SC-ARM-TR-183.

Jensen, MP, JH Flynn, P Kollias, C Kuang, G McFarquhar, H Powers, S Brooks, E Bruning, D Collins, SM Collis, J Fan, A Fridlind, SE Giangrande, R Griffin, J Hu, RC Jackson, M Kumjian, T Logan, T Matsui, CJ Nowotarski, M Oue, AD Rapp, D Rosenfeld, A Ryzhkov, R Sheesley, J Snyder, P Stier, S Usenko, SC van den Heever, M van Lier-Walqui, A Varble, Y Wang, A Aiken, M Deng, D Dexheimer, M Dubey, Y Feng, VP Ghate, KL Johnson, K Lamer, SM Saleeby, D Wang, MA Zawadowicz, and A Zhou. 2023. Tracking Aerosol Convection Interactions Experiment (TRACER) Field Campaign Report. United States. Atmospheric Radiation Measurement user facility, Richland, Washington. DOE/SC-ARM-23-038. https://doi.org/10.2172/2202672

Kay, JE, T L'Ecuyer, A Pendergrass, H Chepfer, R Guzman, and V Yettella. 2018. "Scale-Aware and Definition-Aware Evaluation of Modeled Near-Surface Precipitation Frequency Using CloudSat Observations." *Journal of Geophysical Research – Atmospheres* 123(8): 4294–4309, https://doi.org/10.1002/2017JD028213

McCoy, DT, DL Hartmann, MD Zelinka, P Ceppi, and DP Grosvenor. 2015. "Mixed-Phase Cloud Physics and Southern Ocean Cloud Feedback in Climate Models." *Journal of Geophysical Research – Atmospheres* 120(18): 9539–9554, https://doi.org/10.1002/2015JD023603

Pauley, PM, and X Wu. 1990. "The Theoretical, Discrete, and Actual Response of the Barnes Objective Analysis Scheme for One- and Two-Dimensional Fields." *Monthly Weather Review* 118(5): 1145–1164, https://doi.org/10.1175/1520-0493(1990)118<1145:TTDAAR>2.0.CO;2

Silber, I, RC Jackson, AM Fridlind, AS Ackerman, S Collis, J Verlinde, and J Ding. 2022. "The Earth Model Column Collaboratory (EMC^2) v1.1: An Open-Source Ground-Based Lidar and Radar Instrument Simulator and Subcolumn Generator for Large-Scale Models." *Geoscientific Model Development* 15(2): 901–927, https://doi.org/10.5194/gmd-15-901-2022

Song, H, Z Zhang, P-L Ma, S Ghan, and Mi Wang. 2018. "The Importance of Considering Sub-Grid Cloud Variability When Using Satellite Observations to Evaluate the Cloud and Precipitation Simulations in Climate Models." *Geoscientific Model Development* 11(8): 3147–3158, https://doi.org/10.5194/gmd-11-3147-2018

van der Walt, S, JL Schönberger, J Nunez-Iglesias, F Boulogne, JD Warner, N Yager, E Gouillart, T Yu, and the scikit-image contributors. 2014. "scikit-image: image processing in Python" edited by S. Gomez. *PeerJ* 2: e453, https://doi.org/10.7717/peerj.453

Widener, KB, N Bharadwaj, and K Johnson. 2012. Ka-Band ARM Zenith Radar (KAZR) Handbook. Atmospheric Radiation Measurement user facility, Richland, Washington. DOE/SC-ARM-TR-106.

Appendix A

Feature Statistics Output File

```
netcdf anxkasacrppihydfeatM1.c1.20200313.000000 {
dimensions:
	time = UNLIMITED ; // (1 currently)
	feature_num = 9791 ;
variables:
	int frame(feature_num) ;
		frame:_FillValue = -9999 ;
		frame:long_name = "Field time step (radar ppi) index per sweep in tobac output" ;
		frame:units = "1" ;
	int idx(feature_num) ;
		idx:_FillValue = -9999 ;
		idx:long_name = "Field number index in tobac output (prior to internal concatenation)" ;
		idx:units = "1" ;
	double hdim_1(feature_num) ;
		hdim_1:_FillValue = -9999. ;
		hdim_1:long_name = "Field index dim 1 in tobac output (prior to internal concatenation)"
;
		hdim_1:units = "1" ;
	double hdim_2(feature_num) ;
		hdim_2:_FillValue = -9999. ;
		hdim_2:long_name = "Field index dim 2 in tobac output (prior to internal concatenation)"
;
		hdim_2:units = "1" ;
	int num(feature_num) ;
		num:_FillValue = -9999 ;
		num:long_name = "Pixel numbers in initial tobac output (prior to internal concatenation)"
;
		num:units = "1" ;
	double threshold_value(feature_num) ;
		threshold_value:_FillValue = -9999. ;
		threshold_value:long_name = "Ze threshold applied by tobac to detect hydrometeor field
center" ;
		threshold_value:units = "dBZ" ;
	int feature(feature_num) ;
```

```
		feature:_FillValue = -9999 ;
		feature:long_name = "Feature (detected hydrometeor field) number" ;
		feature:units = "1" ;
	double projection_y_coordinate(feature_num) ;
		projection_y_coordinate:_FillValue = -9999. ;
		projection_y_coordinate:long_name = "Field y coordinate in tobac output (prior to internal concatenation)" ;
		projection_y_coordinate:units = "m" ;
	double projection_x_coordinate(feature_num) ;
		projection_x_coordinate:_FillValue = -9999. ;
		projection_x_coordinate:long_name = "Field x coordinate in tobac output (prior to internal concatenation)" ;
		projection_x_coordinate:units = "m" ;
	double ncells(feature_num) ;
		ncells:_FillValue = -9999. ;
		ncells:long_name = "Pixel count in tobac output (prior to internal concatenation)" ;
		ncells:units = "1" ;
	short edge_flag(feature_num) ;
		edge_flag:_FillValue = -9999s ;
		edge_flag:long_name = "0 - hydrometeor field fully within radar FOV; 1 - hydrometeor field extends beyond the radar FOV" ;
		edge_flag:units = "1" ;
	short V_D_dealiased_flag(feature_num) ;
		V_D_dealiased_flag:_FillValue = -9999s ;
		V_D_dealiased_flag:long_name = "0 - dealiasing not applied (V_D < Nyquist velocity); 1 - dealiasing applied" ;
		V_D_dealiased_flag:units = "1" ;
	double artifact_interp_fraction(feature_num) ;
		artifact_interp_fraction:_FillValue = -9999. ;
		artifact_interp_fraction:long_name = "Fraction of feature pixels included in artifact mask" ;
		artifact_interp_fraction:units = "1" ;
	short artifact_frac_flag(feature_num) ;
		artifact_frac_flag:_FillValue = -9999s ;
		artifact_frac_flag:long_name = "Fraction of artifact-containing pixels exceeds 10% of total feature pixels" ;
		artifact_frac_flag:units = "1" ;
	double V_D_cld_std_std(feature_num) ;
		V_D_cld_std_std:_FillValue = -9999. ;
		V_D_cld_std_std:analysis_type = "values" ;
		V_D_cld_std_std:units = "m/s" ;
		V_D_cld_std_std:long_name = "$V_D$ standard deviation" ;
		V_D_cld_std_std:statistic = "std" ;
	double Ze_mean(feature_num) ;
		Ze_mean:_FillValue = -9999. ;
		Ze_mean:analysis_type = "values" ;
```

```
        Ze_mean:units = "dBZ" ;
        Ze_mean:long_name = "Reflectivity" ;
        Ze_mean:statistic = "mean" ;
    double Ze_std(feature_num) ;
        Ze_std:_FillValue = -9999. ;
        Ze_std:analysis_type = "values" ;
        Ze_std:units = "dBZ" ;
        Ze_std:long_name = "Reflectivity" ;
        Ze_std:statistic = "std" ;
    double Ze_skewness(feature_num) ;
        Ze_skewness:_FillValue = -9999. ;
        Ze_skewness:analysis_type = "values" ;
        Ze_skewness:units = "dBZ" ;
        Ze_skewness:long_name = "Reflectivity" ;
        Ze_skewness:statistic = "skewness" ;
    double Ze_kurtosis(feature_num) ;
        Ze_kurtosis:_FillValue = -9999. ;
        Ze_kurtosis:analysis_type = "values" ;
        Ze_kurtosis:units = "dBZ" ;
        Ze_kurtosis:long_name = "Reflectivity" ;
        Ze_kurtosis:statistic = "kurtosis" ;
    double Ze_min(feature_num) ;
        Ze_min:_FillValue = -9999. ;
        Ze_min:analysis_type = "values" ;
        Ze_min:units = "dBZ" ;
        Ze_min:long_name = "Reflectivity" ;
        Ze_min:statistic = "min" ;
    double Ze_max(feature_num) ;
        Ze_max:_FillValue = -9999. ;
        Ze_max:analysis_type = "values" ;
        Ze_max:units = "dBZ" ;
        Ze_max:long_name = "Reflectivity" ;
        Ze_max:statistic = "max" ;
    double Ze_p01(feature_num) ;
        Ze_p01:_FillValue = -9999. ;
        Ze_p01:analysis_type = "values" ;
        Ze_p01:units = "dBZ" ;
        Ze_p01:long_name = "Reflectivity" ;
        Ze_p01:statistic = "p01" ;
    double Ze_p10(feature_num) ;
        Ze_p10:_FillValue = -9999. ;
        Ze_p10:analysis_type = "values" ;
        Ze_p10:units = "dBZ" ;
        Ze_p10:long_name = "Reflectivity" ;
        Ze_p10:statistic = "p10" ;
    double Ze_p25(feature_num) ;
```

```
        Ze_p25:_FillValue = -9999. ;
        Ze_p25:analysis_type = "values" ;
        Ze_p25:units = "dBZ" ;
        Ze_p25:long_name = "Reflectivity" ;
        Ze_p25:statistic = "p25" ;
    double Ze_p50(feature_num) ;
        Ze_p50:_FillValue = -9999. ;
        Ze_p50:analysis_type = "values" ;
        Ze_p50:units = "dBZ" ;
        Ze_p50:long_name = "Reflectivity" ;
        Ze_p50:statistic = "p50" ;
    double Ze_p75(feature_num) ;
        Ze_p75:_FillValue = -9999. ;
        Ze_p75:analysis_type = "values" ;
        Ze_p75:units = "dBZ" ;
        Ze_p75:long_name = "Reflectivity" ;
        Ze_p75:statistic = "p75" ;
    double Ze_p90(feature_num) ;
        Ze_p90:_FillValue = -9999. ;
        Ze_p90:analysis_type = "values" ;
        Ze_p90:units = "dBZ" ;
        Ze_p90:long_name = "Reflectivity" ;
        Ze_p90:statistic = "p90" ;
    double Ze_p99(feature_num) ;
        Ze_p99:_FillValue = -9999. ;
        Ze_p99:analysis_type = "values" ;
        Ze_p99:units = "dBZ" ;
        Ze_p99:long_name = "Reflectivity" ;
        Ze_p99:statistic = "p99" ;
    double sigma_D_mean(feature_num) ;
        sigma_D_mean:_FillValue = -9999. ;
        sigma_D_mean:analysis_type = "values" ;
        sigma_D_mean:units = "m/s" ;
        sigma_D_mean:long_name = "Doppler spectral width" ;
        sigma_D_mean:statistic = "mean" ;
    double sigma_D_std(feature_num) ;
        sigma_D_std:_FillValue = -9999. ;
        sigma_D_std:analysis_type = "values" ;
        sigma_D_std:units = "m/s" ;
        sigma_D_std:long_name = "Doppler spectral width" ;
        sigma_D_std:statistic = "std" ;
    double sigma_D_skewness(feature_num) ;
        sigma_D_skewness:_FillValue = -9999. ;
        sigma_D_skewness:analysis_type = "values" ;
        sigma_D_skewness:units = "m/s" ;
        sigma_D_skewness:long_name = "Doppler spectral width" ;
```

```
            sigma_D_skewness:statistic = "skewness" ;
    double sigma_D_kurtosis(feature_num) ;
            sigma_D_kurtosis:_FillValue = -9999. ;
            sigma_D_kurtosis:analysis_type = "values" ;
            sigma_D_kurtosis:units = "m/s" ;
            sigma_D_kurtosis:long_name = "Doppler spectral width" ;
            sigma_D_kurtosis:statistic = "kurtosis" ;
    double sigma_D_min(feature_num) ;
            sigma_D_min:_FillValue = -9999. ;
            sigma_D_min:analysis_type = "values" ;
            sigma_D_min:units = "m/s" ;
            sigma_D_min:long_name = "Doppler spectral width" ;
            sigma_D_min:statistic = "min" ;
    double sigma_D_max(feature_num) ;
            sigma_D_max:_FillValue = -9999. ;
            sigma_D_max:analysis_type = "values" ;
            sigma_D_max:units = "m/s" ;
            sigma_D_max:long_name = "Doppler spectral width" ;
            sigma_D_max:statistic = "max" ;
    double sigma_D_p01(feature_num) ;
            sigma_D_p01:_FillValue = -9999. ;
            sigma_D_p01:analysis_type = "values" ;
            sigma_D_p01:units = "m/s" ;
            sigma_D_p01:long_name = "Doppler spectral width" ;
            sigma_D_p01:statistic = "p01" ;
    double sigma_D_p10(feature_num) ;
            sigma_D_p10:_FillValue = -9999. ;
            sigma_D_p10:analysis_type = "values" ;
            sigma_D_p10:units = "m/s" ;
            sigma_D_p10:long_name = "Doppler spectral width" ;
            sigma_D_p10:statistic = "p10" ;
    double sigma_D_p25(feature_num) ;
            sigma_D_p25:_FillValue = -9999. ;
            sigma_D_p25:analysis_type = "values" ;
            sigma_D_p25:units = "m/s" ;
            sigma_D_p25:long_name = "Doppler spectral width" ;
            sigma_D_p25:statistic = "p25" ;
    double sigma_D_p50(feature_num) ;
            sigma_D_p50:_FillValue = -9999. ;
            sigma_D_p50:analysis_type = "values" ;
            sigma_D_p50:units = "m/s" ;
            sigma_D_p50:long_name = "Doppler spectral width" ;
            sigma_D_p50:statistic = "p50" ;
    double sigma_D_p75(feature_num) ;
            sigma_D_p75:_FillValue = -9999. ;
            sigma_D_p75:analysis_type = "values" ;
```

```
		sigma_D_p75:units = "m/s" ;
		sigma_D_p75:long_name = "Doppler spectral width" ;
		sigma_D_p75:statistic = "p75" ;
	double sigma_D_p90(feature_num) ;
		sigma_D_p90:_FillValue = -9999. ;
		sigma_D_p90:analysis_type = "values" ;
		sigma_D_p90:units = "m/s" ;
		sigma_D_p90:long_name = "Doppler spectral width" ;
		sigma_D_p90:statistic = "p90" ;
	double sigma_D_p99(feature_num) ;
		sigma_D_p99:_FillValue = -9999. ;
		sigma_D_p99:analysis_type = "values" ;
		sigma_D_p99:units = "m/s" ;
		sigma_D_p99:long_name = "Doppler spectral width" ;
		sigma_D_p99:statistic = "p99" ;
	double SR_Silber2023_mean(feature_num) ;
		SR_Silber2023_mean:_FillValue = -9999. ;
		SR_Silber2023_mean:analysis_type = "Z-S_Silber2023" ;
		SR_Silber2023_mean:units = "mm/h" ;
		SR_Silber2023_mean:long_name = "Snow rate (cloud base; Silber, 2023)" ;
		SR_Silber2023_mean:database = "Cloud base; ARM NSA site; KAZR/HSRL/SONDE" ;
		SR_Silber2023_mean:source = "Their Table 3" ;
		SR_Silber2023_mean:reference = "https://doi.org/10.1029/2022JD038202" ;
		SR_Silber2023_mean:statistic = "mean" ;
	double SR_Silber2023_std(feature_num) ;
		SR_Silber2023_std:_FillValue = -9999. ;
		SR_Silber2023_std:analysis_type = "Z-S_Silber2023" ;
		SR_Silber2023_std:units = "mm/h" ;
		SR_Silber2023_std:long_name = "Snow rate (cloud base; Silber, 2023)" ;
		SR_Silber2023_std:database = "Cloud base; ARM NSA site; KAZR/HSRL/SONDE" ;
		SR_Silber2023_std:source = "Their Table 3" ;
		SR_Silber2023_std:reference = "https://doi.org/10.1029/2022JD038202" ;
		SR_Silber2023_std:statistic = "std" ;
	double SR_Silber2023_p99(feature_num) ;
		SR_Silber2023_p99:_FillValue = -9999. ;
		SR_Silber2023_p99:analysis_type = "Z-S_Silber2023" ;
		SR_Silber2023_p99:units = "mm/h" ;
		SR_Silber2023_p99:long_name = "Snow rate (cloud base; Silber, 2023)" ;
		SR_Silber2023_p99:database = "Cloud base; ARM NSA site; KAZR/HSRL/SONDE" ;
		SR_Silber2023_p99:source = "Their Table 3" ;
		SR_Silber2023_p99:reference = "https://doi.org/10.1029/2022JD038202" ;
		SR_Silber2023_p99:statistic = "p99" ;
	double SR_Souverijns2017_mean(feature_num) ;
		SR_Souverijns2017_mean:_FillValue = -9999. ;
		SR_Souverijns2017_mean:analysis_type = "Z-R" ;
		SR_Souverijns2017_mean:a = 18. ;
```

```
        SR_Souverijns2017_mean:b = 1.1 ;
        SR_Souverijns2017_mean:units = "mm/h" ;
        SR_Souverijns2017_mean:long_name = "Snow rate (surface; Souverijns et al., 2017)" ;
        SR_Souverijns2017_mean:database = "Surface; Princess Elisabeth, Antarctica;
PIP/MRR" ;
        SR_Souverijns2017_mean:source = "Their Text" ;
        SR_Souverijns2017_mean:reference = "https://doi.org/10.1016/j.atmosres.2017.06.001" ;
        SR_Souverijns2017_mean:statistic = "mean" ;
    double SR_Souverijns2017_std(feature_num) ;
        SR_Souverijns2017_std:_FillValue = -9999. ;
        SR_Souverijns2017_std:analysis_type = "Z-R" ;
        SR_Souverijns2017_std:a = 18. ;
        SR_Souverijns2017_std:b = 1.1 ;
        SR_Souverijns2017_std:units = "mm/h" ;
        SR_Souverijns2017_std:long_name = "Snow rate (surface; Souverijns et al., 2017)" ;
        SR_Souverijns2017_std:database = "Surface; Princess Elisabeth, Antarctica; PIP/MRR" ;
        SR_Souverijns2017_std:source = "Their Text" ;
        SR_Souverijns2017_std:reference = "https://doi.org/10.1016/j.atmosres.2017.06.001" ;
        SR_Souverijns2017_std:statistic = "std" ;
    double SR_Souverijns2017_p99(feature_num) ;
        SR_Souverijns2017_p99:_FillValue = -9999. ;
        SR_Souverijns2017_p99:analysis_type = "Z-R" ;
        SR_Souverijns2017_p99:a = 18. ;
        SR_Souverijns2017_p99:b = 1.1 ;
        SR_Souverijns2017_p99:units = "mm/h" ;
        SR_Souverijns2017_p99:long_name = "Snow rate (surface; Souverijns et al., 2017)" ;
        SR_Souverijns2017_p99:database = "Surface; Princess Elisabeth, Antarctica; PIP/MRR"
;
        SR_Souverijns2017_p99:source = "Their Text" ;
        SR_Souverijns2017_p99:reference = "https://doi.org/10.1016/j.atmosres.2017.06.001" ;
        SR_Souverijns2017_p99:statistic = "p99" ;
    double SR_KulieBennartz2009_mean(feature_num) ;
        SR_KulieBennartz2009_mean:_FillValue = -9999. ;
        SR_KulieBennartz2009_mean:analysis_type = "Z-S_KuliBennartz2009" ;
        SR_KulieBennartz2009_mean:units = "mm/h" ;
        SR_KulieBennartz2009_mean:long_name = "Snow rate (aggregates model; Kulie and
Bennartz, 2009)" ;
        SR_KulieBennartz2009_mean:database = "Ice habit models" ;
        SR_KulieBennartz2009_mean:source = "Their Table 1 (HA category)" ;
        SR_KulieBennartz2009_mean:reference = "https://doi.org/10.1175/2009JAMC2193.1" ;
        SR_KulieBennartz2009_mean:statistic = "mean" ;
    double SR_KulieBennartz2009_std(feature_num) ;
        SR_KulieBennartz2009_std:_FillValue = -9999. ;
        SR_KulieBennartz2009_std:analysis_type = "Z-S_KuliBennartz2009" ;
        SR_KulieBennartz2009_std:units = "mm/h" ;
```

```
                SR_KulieBennartz2009_std:long_name = "Snow rate (aggregates model; Kulie and
Bennartz, 2009)" ;
                SR_KulieBennartz2009_std:database = "Ice habit models" ;
                SR_KulieBennartz2009_std:source = "Their Table 1 (HA category)" ;
                SR_KulieBennartz2009_std:reference = "https://doi.org/10.1175/2009JAMC2193.1" ;
                SR_KulieBennartz2009_std:statistic = "std" ;
        double SR_KulieBennartz2009_p99(feature_num) ;
                SR_KulieBennartz2009_p99:_FillValue = -9999. ;
                SR_KulieBennartz2009_p99:analysis_type = "Z-S_KuliBennartz2009" ;
                SR_KulieBennartz2009_p99:units = "mm/h" ;
                SR_KulieBennartz2009_p99:long_name = "Snow rate (aggregates model; Kulie and
Bennartz, 2009)" ;
                SR_KulieBennartz2009_p99:database = "Ice habit models" ;
                SR_KulieBennartz2009_p99:source = "Their Table 1 (HA category)" ;
                SR_KulieBennartz2009_p99:reference = "https://doi.org/10.1175/2009JAMC2193.1" ;
                SR_KulieBennartz2009_p99:statistic = "p99" ;
        double SR_Matrosov2007_mean(feature_num) ;
                SR_Matrosov2007_mean:_FillValue = -9999. ;
                SR_Matrosov2007_mean:analysis_type = "Z-S_Matrosov2007" ;
                SR_Matrosov2007_mean:units = "mm/h" ;
                SR_Matrosov2007_mean:long_name = "Snow rate (ice models; Matrosov, 2007)" ;
                SR_Matrosov2007_mean:database = "Ice habit models" ;
                SR_Matrosov2007_mean:source = "Their Table 1" ;
                SR_Matrosov2007_mean:reference = "https://doi.org/10.1175/JAS3904.1" ;
                SR_Matrosov2007_mean:statistic = "mean" ;
        double SR_Matrosov2007_std(feature_num) ;
                SR_Matrosov2007_std:_FillValue = -9999. ;
                SR_Matrosov2007_std:analysis_type = "Z-S_Matrosov2007" ;
                SR_Matrosov2007_std:units = "mm/h" ;
                SR_Matrosov2007_std:long_name = "Snow rate (ice models; Matrosov, 2007)" ;
                SR_Matrosov2007_std:database = "Ice habit models" ;
                SR_Matrosov2007_std:source = "Their Table 1" ;
                SR_Matrosov2007_std:reference = "https://doi.org/10.1175/JAS3904.1" ;
                SR_Matrosov2007_std:statistic = "std" ;
        double SR_Matrosov2007_p99(feature_num) ;
                SR_Matrosov2007_p99:_FillValue = -9999. ;
                SR_Matrosov2007_p99:analysis_type = "Z-S_Matrosov2007" ;
                SR_Matrosov2007_p99:units = "mm/h" ;
                SR_Matrosov2007_p99:long_name = "Snow rate (ice models; Matrosov, 2007)" ;
                SR_Matrosov2007_p99:database = "Ice habit models" ;
                SR_Matrosov2007_p99:source = "Their Table 1" ;
                SR_Matrosov2007_p99:reference = "https://doi.org/10.1175/JAS3904.1" ;
                SR_Matrosov2007_p99:statistic = "p99" ;
        double SR_Heymsfield2018_mean(feature_num) ;
                SR_Heymsfield2018_mean:_FillValue = -9999. ;
                SR_Heymsfield2018_mean:analysis_type = "Z-S_Heymsfield2018" ;
```

```
		SR_Heymsfield2018_mean:units = "mm/h" ;
		SR_Heymsfield2018_mean:long_name = "Snow rate (in-cloud; Heymsfield et al., 2018)" ;
		SR_Heymsfield2018_mean:database = "In-cloud; Washington State (OLYMPEX) and Ontario, Canada GCPEX; 2D-S/HVPS-3/APR-3/APR-2/2D-C/CIP" ;
		SR_Heymsfield2018_mean:source = "Their Table 3 for no liquid water cases" ;
		SR_Heymsfield2018_mean:reference = "https://doi.org/10.1175/JAMC-D-17-0164.1" ;
		SR_Heymsfield2018_mean:statistic = "mean" ;
	double SR_Heymsfield2018_std(feature_num) ;
		SR_Heymsfield2018_std:_FillValue = -9999. ;
		SR_Heymsfield2018_std:analysis_type = "Z-S_Heymsfield2018" ;
		SR_Heymsfield2018_std:units = "mm/h" ;
		SR_Heymsfield2018_std:long_name = "Snow rate (in-cloud; Heymsfield et al., 2018)" ;
		SR_Heymsfield2018_std:database = "In-cloud; Washington State (OLYMPEX) and Ontario, Canada GCPEX; 2D-S/HVPS-3/APR-3/APR-2/2D-C/CIP" ;
		SR_Heymsfield2018_std:source = "Their Table 3 for no liquid water cases" ;
		SR_Heymsfield2018_std:reference = "https://doi.org/10.1175/JAMC-D-17-0164.1" ;
		SR_Heymsfield2018_std:statistic = "std" ;
	double SR_Heymsfield2018_p99(feature_num) ;
		SR_Heymsfield2018_p99:_FillValue = -9999. ;
		SR_Heymsfield2018_p99:analysis_type = "Z-S_Heymsfield2018" ;
		SR_Heymsfield2018_p99:units = "mm/h" ;
		SR_Heymsfield2018_p99:long_name = "Snow rate (in-cloud; Heymsfield et al., 2018)" ;
		SR_Heymsfield2018_p99:database = "In-cloud; Washington State (OLYMPEX) and Ontario, Canada GCPEX; 2D-S/HVPS-3/APR-3/APR-2/2D-C/CIP" ;
		SR_Heymsfield2018_p99:source = "Their Table 3 for no liquid water cases" ;
		SR_Heymsfield2018_p99:reference = "https://doi.org/10.1175/JAMC-D-17-0164.1" ;
		SR_Heymsfield2018_p99:statistic = "p99" ;
	double SR_LR_Falconi2018_mean(feature_num) ;
		SR_LR_Falconi2018_mean:_FillValue = -9999. ;
		SR_LR_Falconi2018_mean:analysis_type = "Z-S_LR_Falconi2018" ;
		SR_LR_Falconi2018_mean:units = "mm/h" ;
		SR_LR_Falconi2018_mean:long_name = "Snow rate (surface; Falconi et al., 2018)" ;
		SR_LR_Falconi2018_mean:database = "Surface; Hyytiälä, Finland BAECC; PIP/Pluvio/MWR/KAZR/MWACR/XSACR" ;
		SR_LR_Falconi2018_mean:source = "Their Table 2 for light riming" ;
		SR_LR_Falconi2018_mean:reference = "https://doi.org/10.5194/amt-11-3059-2018" ;
		SR_LR_Falconi2018_mean:statistic = "mean" ;
	double SR_LR_Falconi2018_std(feature_num) ;
		SR_LR_Falconi2018_std:_FillValue = -9999. ;
		SR_LR_Falconi2018_std:analysis_type = "Z-S_LR_Falconi2018" ;
		SR_LR_Falconi2018_std:units = "mm/h" ;
		SR_LR_Falconi2018_std:long_name = "Snow rate (surface; Falconi et al., 2018)" ;
		SR_LR_Falconi2018_std:database = "Surface; Hyytiälä, Finland BAECC; PIP/Pluvio/MWR/KAZR/MWACR/XSACR" ;
		SR_LR_Falconi2018_std:source = "Their Table 2 for light riming" ;
```

SR_LR_Falconi2018_std:reference = "https://doi.org/10.5194/amt-11-3059-2018" ;
SR_LR_Falconi2018_std:statistic = "std" ;
double SR_LR_Falconi2018_p99(feature_num) ;
SR_LR_Falconi2018_p99:_FillValue = -9999. ;
SR_LR_Falconi2018_p99:analysis_type = "Z-S_LR_Falconi2018" ;
SR_LR_Falconi2018_p99:units = "mm/h" ;
SR_LR_Falconi2018_p99:long_name = "Snow rate (surface; Falconi et al., 2018)" ;
SR_LR_Falconi2018_p99:database = "Surface; Hyytiälä, Finland BAECC; PIP/Pluvio/MWR/KAZR/MWACR/XSACR" ;
SR_LR_Falconi2018_p99:source = "Their Table 2 for light riming" ;
SR_LR_Falconi2018_p99:reference = "https://doi.org/10.5194/amt-11-3059-2018" ;
SR_LR_Falconi2018_p99:statistic = "p99" ;
double SR_MR_Falconi2018_mean(feature_num) ;
SR_MR_Falconi2018_mean:_FillValue = -9999. ;
SR_MR_Falconi2018_mean:analysis_type = "Z-S_MR_Falconi2018" ;
SR_MR_Falconi2018_mean:units = "mm/h" ;
SR_MR_Falconi2018_mean:long_name = "Snow rate (surface; Falconi et al., 2018)" ;
SR_MR_Falconi2018_mean:database = "Surface; Hyytiälä, Finland BAECC; PIP/Pluvio/MWR/KAZR/MWACR/XSACR" ;
SR_MR_Falconi2018_mean:source = "Their Table 2 for moderate riming" ;
SR_MR_Falconi2018_mean:reference = "https://doi.org/10.5194/amt-11-3059-2018" ;
SR_MR_Falconi2018_mean:statistic = "mean" ;
double SR_MR_Falconi2018_std(feature_num) ;
SR_MR_Falconi2018_std:_FillValue = -9999. ;
SR_MR_Falconi2018_std:analysis_type = "Z-S_MR_Falconi2018" ;
SR_MR_Falconi2018_std:units = "mm/h" ;
SR_MR_Falconi2018_std:long_name = "Snow rate (surface; Falconi et al., 2018)" ;
SR_MR_Falconi2018_std:database = "Surface; Hyytiälä, Finland BAECC; PIP/Pluvio/MWR/KAZR/MWACR/XSACR" ;
SR_MR_Falconi2018_std:source = "Their Table 2 for moderate riming" ;
SR_MR_Falconi2018_std:reference = "https://doi.org/10.5194/amt-11-3059-2018" ;
SR_MR_Falconi2018_std:statistic = "std" ;
double SR_MR_Falconi2018_p99(feature_num) ;
SR_MR_Falconi2018_p99:_FillValue = -9999. ;
SR_MR_Falconi2018_p99:analysis_type = "Z-S_MR_Falconi2018" ;
SR_MR_Falconi2018_p99:units = "mm/h" ;
SR_MR_Falconi2018_p99:long_name = "Snow rate (surface; Falconi et al., 2018)" ;
SR_MR_Falconi2018_p99:database = "Surface; Hyytiälä, Finland BAECC; PIP/Pluvio/MWR/KAZR/MWACR/XSACR" ;
SR_MR_Falconi2018_p99:source = "Their Table 2 for moderate riming" ;
SR_MR_Falconi2018_p99:reference = "https://doi.org/10.5194/amt-11-3059-2018" ;
SR_MR_Falconi2018_p99:statistic = "p99" ;
double IWC_Silber2023_mean(feature_num) ;
IWC_Silber2023_mean:_FillValue = -9999. ;
IWC_Silber2023_mean:analysis_type = "Z-IWC_Silber2023" ;
IWC_Silber2023_mean:units = "g/m^3" ;

```
                IWC_Silber2023_mean:long_name = "IWC (cloud base; Silber, 2023)" ;
                IWC_Silber2023_mean:database = "Cloud base; ARM NSA site; KAZR/HSRL/SONDE"
;
                IWC_Silber2023_mean:source = "Their Table 3" ;
                IWC_Silber2023_mean:reference = "https://doi.org/10.1029/2022JD038202" ;
                IWC_Silber2023_mean:statistic = "mean" ;
        double IWC_Silber2023_std(feature_num) ;
                IWC_Silber2023_std:_FillValue = -9999. ;
                IWC_Silber2023_std:analysis_type = "Z-IWC_Silber2023" ;
                IWC_Silber2023_std:units = "g/m^3" ;
                IWC_Silber2023_std:long_name = "IWC (cloud base; Silber, 2023)" ;
                IWC_Silber2023_std:database = "Cloud base; ARM NSA site; KAZR/HSRL/SONDE" ;
                IWC_Silber2023_std:source = "Their Table 3" ;
                IWC_Silber2023_std:reference = "https://doi.org/10.1029/2022JD038202" ;
                IWC_Silber2023_std:statistic = "std" ;
        double IWC_Silber2023_p99(feature_num) ;
                IWC_Silber2023_p99:_FillValue = -9999. ;
                IWC_Silber2023_p99:analysis_type = "Z-IWC_Silber2023" ;
                IWC_Silber2023_p99:units = "g/m^3" ;
                IWC_Silber2023_p99:long_name = "IWC (cloud base; Silber, 2023)" ;
                IWC_Silber2023_p99:database = "Cloud base; ARM NSA site; KAZR/HSRL/SONDE" ;
                IWC_Silber2023_p99:source = "Their Table 3" ;
                IWC_Silber2023_p99:reference = "https://doi.org/10.1029/2022JD038202" ;
                IWC_Silber2023_p99:statistic = "p99" ;
        double IWC_Heymsfield2018_mean(feature_num) ;
                IWC_Heymsfield2018_mean:_FillValue = -9999. ;
                IWC_Heymsfield2018_mean:analysis_type = "R-ZdBZ" ;
                IWC_Heymsfield2018_mean:a = 0.297 ;
                IWC_Heymsfield2018_mean:b = 0.151 ;
                IWC_Heymsfield2018_mean:units = "g/m^3" ;
                IWC_Heymsfield2018_mean:long_name = "IWC (in-cloud; Heymsfield et al., 2018)" ;
                IWC_Heymsfield2018_mean:database = "In-cloud; Washington State (OLYMPEX) and
Ontario, Canada GCPEX; 2D-S/HVPS-3/APR-3/APR-2/2D-C/CIP" ;
                IWC_Heymsfield2018_mean:source = "Their Table 3 composite" ;
                IWC_Heymsfield2018_mean:reference = "https://doi.org/10.1175/JAMC-D-17-0164.1" ;
                IWC_Heymsfield2018_mean:statistic = "mean" ;
        double IWC_Heymsfield2018_std(feature_num) ;
                IWC_Heymsfield2018_std:_FillValue = -9999. ;
                IWC_Heymsfield2018_std:analysis_type = "R-ZdBZ" ;
                IWC_Heymsfield2018_std:a = 0.297 ;
                IWC_Heymsfield2018_std:b = 0.151 ;
                IWC_Heymsfield2018_std:units = "g/m^3" ;
                IWC_Heymsfield2018_std:long_name = "IWC (in-cloud; Heymsfield et al., 2018)" ;
                IWC_Heymsfield2018_std:database = "In-cloud; Washington State (OLYMPEX) and
Ontario, Canada GCPEX; 2D-S/HVPS-3/APR-3/APR-2/2D-C/CIP" ;
                IWC_Heymsfield2018_std:source = "Their Table 3 composite" ;
```

```
        IWC_Heymsfield2018_std:reference = "https://doi.org/10.1175/JAMC-D-17-0164.1" ;
        IWC_Heymsfield2018_std:statistic = "std" ;
    double IWC_Heymsfield2018_p99(feature_num) ;
        IWC_Heymsfield2018_p99:_FillValue = -9999. ;
        IWC_Heymsfield2018_p99:analysis_type = "R-ZdBZ" ;
        IWC_Heymsfield2018_p99:a = 0.297 ;
        IWC_Heymsfield2018_p99:b = 0.151 ;
        IWC_Heymsfield2018_p99:units = "g/m^3" ;
        IWC_Heymsfield2018_p99:long_name = "IWC (in-cloud; Heymsfield et al., 2018)" ;
        IWC_Heymsfield2018_p99:database = "In-cloud; Washington State (OLYMPEX) and
Ontario, Canada GCPEX; 2D-S/HVPS-3/APR-3/APR-2/2D-C/CIP" ;
        IWC_Heymsfield2018_p99:source = "Their Table 3 composite" ;
        IWC_Heymsfield2018_p99:reference = "https://doi.org/10.1175/JAMC-D-17-0164.1" ;
        IWC_Heymsfield2018_p99:statistic = "p99" ;
    double IWC_Hogan2006_mean(feature_num) ;
        IWC_Hogan2006_mean:_FillValue = -9999. ;
        IWC_Hogan2006_mean:analysis_type = "ZT-IWC_Hogan2006" ;
        IWC_Hogan2006_mean:units = "g/m^3" ;
        IWC_Hogan2006_mean:long_name = "IWC (ice clouds; Hogan et al., 2006)" ;
        IWC_Hogan2006_mean:database = "Ice clouds; United Kingdom; 2D-C/2D-P" ;
        IWC_Hogan2006_mean:source = "Their Table 2" ;
        IWC_Hogan2006_mean:reference = "https://doi.org/10.1175/JAM2340.1" ;
        IWC_Hogan2006_mean:statistic = "mean" ;
    double IWC_Hogan2006_std(feature_num) ;
        IWC_Hogan2006_std:_FillValue = -9999. ;
        IWC_Hogan2006_std:analysis_type = "ZT-IWC_Hogan2006" ;
        IWC_Hogan2006_std:units = "g/m^3" ;
        IWC_Hogan2006_std:long_name = "IWC (ice clouds; Hogan et al., 2006)" ;
        IWC_Hogan2006_std:database = "Ice clouds; United Kingdom; 2D-C/2D-P" ;
        IWC_Hogan2006_std:source = "Their Table 2" ;
        IWC_Hogan2006_std:reference = "https://doi.org/10.1175/JAM2340.1" ;
        IWC_Hogan2006_std:statistic = "std" ;
    double IWC_Hogan2006_p99(feature_num) ;
        IWC_Hogan2006_p99:_FillValue = -9999. ;
        IWC_Hogan2006_p99:analysis_type = "ZT-IWC_Hogan2006" ;
        IWC_Hogan2006_p99:units = "g/m^3" ;
        IWC_Hogan2006_p99:long_name = "IWC (ice clouds; Hogan et al., 2006)" ;
        IWC_Hogan2006_p99:database = "Ice clouds; United Kingdom; 2D-C/2D-P" ;
        IWC_Hogan2006_p99:source = "Their Table 2" ;
        IWC_Hogan2006_p99:reference = "https://doi.org/10.1175/JAM2340.1" ;
        IWC_Hogan2006_p99:statistic = "p99" ;
    double RR_Comstock2004_CB_mean(feature_num) ;
        RR_Comstock2004_CB_mean:_FillValue = -9999. ;
        RR_Comstock2004_CB_mean:analysis_type = "Z-R" ;
        RR_Comstock2004_CB_mean:a = 25. ;
        RR_Comstock2004_CB_mean:b = 1.3 ;
```

```
		RR_Comstock2004_CB_mean:units = "mm/h" ;
		RR_Comstock2004_CB_mean:long_name = "Rain rate (cloud base; Comstock et al.,
2004)" ;
		RR_Comstock2004_CB_mean:database = "Cloud base; East Pacific EPIC Sc; MMCR" ;
		RR_Comstock2004_CB_mean:source = "Their text and Figure 6" ;
		RR_Comstock2004_CB_mean:reference = "https://doi.org/10.1256/qj.03.187" ;
		RR_Comstock2004_CB_mean:statistic = "mean" ;
	double RR_Comstock2004_CB_std(feature_num) ;
		RR_Comstock2004_CB_std:_FillValue = -9999. ;
		RR_Comstock2004_CB_std:analysis_type = "Z-R" ;
		RR_Comstock2004_CB_std:a = 25. ;
		RR_Comstock2004_CB_std:b = 1.3 ;
		RR_Comstock2004_CB_std:units = "mm/h" ;
		RR_Comstock2004_CB_std:long_name = "Rain rate (cloud base; Comstock et al.,
2004)" ;
		RR_Comstock2004_CB_std:database = "Cloud base; East Pacific EPIC Sc; MMCR" ;
		RR_Comstock2004_CB_std:source = "Their text and Figure 6" ;
		RR_Comstock2004_CB_std:reference = "https://doi.org/10.1256/qj.03.187" ;
		RR_Comstock2004_CB_std:statistic = "std" ;
	double RR_Comstock2004_CB_p99(feature_num) ;
		RR_Comstock2004_CB_p99:_FillValue = -9999. ;
		RR_Comstock2004_CB_p99:analysis_type = "Z-R" ;
		RR_Comstock2004_CB_p99:a = 25. ;
		RR_Comstock2004_CB_p99:b = 1.3 ;
		RR_Comstock2004_CB_p99:units = "mm/h" ;
		RR_Comstock2004_CB_p99:long_name = "Rain rate (cloud base; Comstock et al.,
2004)" ;
		RR_Comstock2004_CB_p99:database = "Cloud base; East Pacific EPIC Sc; MMCR" ;
		RR_Comstock2004_CB_p99:source = "Their text and Figure 6" ;
		RR_Comstock2004_CB_p99:reference = "https://doi.org/10.1256/qj.03.187" ;
		RR_Comstock2004_CB_p99:statistic = "p99" ;
	double RR_VanZanten2005_CB_mean(feature_num) ;
		RR_VanZanten2005_CB_mean:_FillValue = -9999. ;
		RR_VanZanten2005_CB_mean:analysis_type = "R-ZdBZ" ;
		RR_VanZanten2005_CB_mean:a = 0.11375 ;
		RR_VanZanten2005_CB_mean:b = 0.68 ;
		RR_VanZanten2005_CB_mean:units = "mm/h" ;
		RR_VanZanten2005_CB_mean:long_name = "Rain rate (cloud base; VanZanten et al.,
2005)" ;
		RR_VanZanten2005_CB_mean:database = "Cloud base; NorthEast Pacific (San Diego)
DYCOMS-II Sc; SPP-100/260x" ;
		RR_VanZanten2005_CB_mean:source = "Their \'All\' category in Table 2; converted
from mm/day to mm/h" ;
		RR_VanZanten2005_CB_mean:reference = "https://doi.org/10.1175/JAS-3355.1" ;
		RR_VanZanten2005_CB_mean:statistic = "mean" ;
	double RR_VanZanten2005_CB_std(feature_num) ;
```

```
                RR_VanZanten2005_CB_std:_FillValue = -9999. ;
                RR_VanZanten2005_CB_std:analysis_type = "R-ZdBZ" ;
                RR_VanZanten2005_CB_std:a = 0.11375 ;
                RR_VanZanten2005_CB_std:b = 0.68 ;
                RR_VanZanten2005_CB_std:units = "mm/h" ;
                RR_VanZanten2005_CB_std:long_name = "Rain rate (cloud base; VanZanten et al.,
2005)" ;
                RR_VanZanten2005_CB_std:database = "Cloud base; NorthEast Pacific (San Diego)
DYCOMS-II Sc; SPP-100/260x" ;
                RR_VanZanten2005_CB_std:source = "Their \'All\' category in Table 2; converted from
mm/day to mm/h" ;
                RR_VanZanten2005_CB_std:reference = "https://doi.org/10.1175/JAS-3355.1" ;
                RR_VanZanten2005_CB_std:statistic = "std" ;
        double RR_VanZanten2005_CB_p99(feature_num) ;
                RR_VanZanten2005_CB_p99:_FillValue = -9999. ;
                RR_VanZanten2005_CB_p99:analysis_type = "R-ZdBZ" ;
                RR_VanZanten2005_CB_p99:a = 0.11375 ;
                RR_VanZanten2005_CB_p99:b = 0.68 ;
                RR_VanZanten2005_CB_p99:units = "mm/h" ;
                RR_VanZanten2005_CB_p99:long_name = "Rain rate (cloud base; VanZanten et al.,
2005)" ;
                RR_VanZanten2005_CB_p99:database = "Cloud base; NorthEast Pacific (San Diego)
DYCOMS-II Sc; SPP-100/260x" ;
                RR_VanZanten2005_CB_p99:source = "Their \'All\' category in Table 2; converted from
mm/day to mm/h" ;
                RR_VanZanten2005_CB_p99:reference = "https://doi.org/10.1175/JAS-3355.1" ;
                RR_VanZanten2005_CB_p99:statistic = "p99" ;
        double RR_VanZanten2005_SFC_mean(feature_num) ;
                RR_VanZanten2005_SFC_mean:_FillValue = -9999. ;
                RR_VanZanten2005_SFC_mean:analysis_type = "R-ZdBZ" ;
                RR_VanZanten2005_SFC_mean:a = 0.02125 ;
                RR_VanZanten2005_SFC_mean:b = 0.34 ;
                RR_VanZanten2005_SFC_mean:units = "mm/h" ;
                RR_VanZanten2005_SFC_mean:long_name = "Rain rate (surface; VanZanten et al.,
2005)" ;
                RR_VanZanten2005_SFC_mean:database = "Surface; NorthEast Pacific (San Diego)
DYCOMS-II Sc; SPP-100/260x" ;
                RR_VanZanten2005_SFC_mean:source = "Their \'All\' category in Table 2; converted
from mm/day to mm/h" ;
                RR_VanZanten2005_SFC_mean:reference = "https://doi.org/10.1175/JAS-3355.1" ;
                RR_VanZanten2005_SFC_mean:statistic = "mean" ;
        double RR_VanZanten2005_SFC_std(feature_num) ;
                RR_VanZanten2005_SFC_std:_FillValue = -9999. ;
                RR_VanZanten2005_SFC_std:analysis_type = "R-ZdBZ" ;
                RR_VanZanten2005_SFC_std:a = 0.02125 ;
                RR_VanZanten2005_SFC_std:b = 0.34 ;
```

RR_VanZanten2005_SFC_std:units = "mm/h" ;
RR_VanZanten2005_SFC_std:long_name = "Rain rate (surface; VanZanten et al., 2005)" ;
RR_VanZanten2005_SFC_std:database = "Surface; NorthEast Pacific (San Diego) DYCOMS-II Sc; SPP-100/260x" ;
RR_VanZanten2005_SFC_std:source = "Their \'All\' category in Table 2; converted from mm/day to mm/h" ;
RR_VanZanten2005_SFC_std:reference = "https://doi.org/10.1175/JAS-3355.1" ;
RR_VanZanten2005_SFC_std:statistic = "std" ;
double RR_VanZanten2005_SFC_p99(feature_num) ;
RR_VanZanten2005_SFC_p99:_FillValue = -9999. ;
RR_VanZanten2005_SFC_p99:analysis_type = "R-ZdBZ" ;
RR_VanZanten2005_SFC_p99:a = 0.02125 ;
RR_VanZanten2005_SFC_p99:b = 0.34 ;
RR_VanZanten2005_SFC_p99:units = "mm/h" ;
RR_VanZanten2005_SFC_p99:long_name = "Rain rate (surface; VanZanten et al., 2005)" ;
RR_VanZanten2005_SFC_p99:database = "Surface; NorthEast Pacific (San Diego) DYCOMS-II Sc; SPP-100/260x" ;
RR_VanZanten2005_SFC_p99:source = "Their \'All\' category in Table 2; converted from mm/day to mm/h" ;
RR_VanZanten2005_SFC_p99:reference = "https://doi.org/10.1175/JAS-3355.1" ;
RR_VanZanten2005_SFC_p99:statistic = "p99" ;
double RR_Wood2005_CLD_mean(feature_num) ;
RR_Wood2005_CLD_mean:_FillValue = -9999. ;
RR_Wood2005_CLD_mean:analysis_type = "Z-R" ;
RR_Wood2005_CLD_mean:a = 12.4 ;
RR_Wood2005_CLD_mean:b = 1.18 ;
RR_Wood2005_CLD_mean:units = "mm/h" ;
RR_Wood2005_CLD_mean:long_name = "Rain rate (in-cloud; Wood, 2005)" ;
RR_Wood2005_CLD_mean:database = "In-cloud; NorthEast Atlantic ASTEX Sc; FSSP/2D-C" ;
RR_Wood2005_CLD_mean:source = "Their Table 2 for exponential (better fit based on text)" ;
RR_Wood2005_CLD_mean:reference = "https://doi.org/10.1175/JAS3530.1" ;
RR_Wood2005_CLD_mean:statistic = "mean" ;
double RR_Wood2005_CLD_std(feature_num) ;
RR_Wood2005_CLD_std:_FillValue = -9999. ;
RR_Wood2005_CLD_std:analysis_type = "Z-R" ;
RR_Wood2005_CLD_std:a = 12.4 ;
RR_Wood2005_CLD_std:b = 1.18 ;
RR_Wood2005_CLD_std:units = "mm/h" ;
RR_Wood2005_CLD_std:long_name = "Rain rate (in-cloud; Wood, 2005)" ;
RR_Wood2005_CLD_std:database = "In-cloud; NorthEast Atlantic ASTEX Sc; FSSP/2D-C" ;

```
                RR_Wood2005_CLD_std:source = "Their Table 2 for exponential (better fit based on
text)" ;
                RR_Wood2005_CLD_std:reference = "https://doi.org/10.1175/JAS3530.1" ;
                RR_Wood2005_CLD_std:statistic = "std" ;
        double RR_Wood2005_CLD_p99(feature_num) ;
                RR_Wood2005_CLD_p99:_FillValue = -9999. ;
                RR_Wood2005_CLD_p99:analysis_type = "Z-R" ;
                RR_Wood2005_CLD_p99:a = 12.4 ;
                RR_Wood2005_CLD_p99:b = 1.18 ;
                RR_Wood2005_CLD_p99:units = "mm/h" ;
                RR_Wood2005_CLD_p99:long_name = "Rain rate (in-cloud; Wood, 2005)" ;
                RR_Wood2005_CLD_p99:database = "In-cloud; NorthEast Atlantic ASTEX Sc;
FSSP/2D-C" ;
                RR_Wood2005_CLD_p99:source = "Their Table 2 for exponential (better fit based on
text)" ;
                RR_Wood2005_CLD_p99:reference = "https://doi.org/10.1175/JAS3530.1" ;
                RR_Wood2005_CLD_p99:statistic = "p99" ;
        double alt_mean(feature_num) ;
                alt_mean:_FillValue = -9999. ;
                alt_mean:analysis_type = "values" ;
                alt_mean:units = "m" ;
                alt_mean:long_name = "Estimated height" ;
                alt_mean:statistic = "mean" ;
        double alt_min(feature_num) ;
                alt_min:_FillValue = -9999. ;
                alt_min:analysis_type = "values" ;
                alt_min:units = "m" ;
                alt_min:long_name = "Estimated height" ;
                alt_min:statistic = "min" ;
        double alt_max(feature_num) ;
                alt_max:_FillValue = -9999. ;
                alt_max:analysis_type = "values" ;
                alt_max:units = "m" ;
                alt_max:long_name = "Estimated height" ;
                alt_max:statistic = "max" ;
        double T_mean(feature_num) ;
                T_mean:_FillValue = -9999. ;
                T_mean:analysis_type = "values" ;
                T_mean:units = "degC" ;
                T_mean:long_name = "Interpolated temperature" ;
                T_mean:statistic = "mean" ;
        double T_min(feature_num) ;
                T_min:_FillValue = -9999. ;
                T_min:analysis_type = "values" ;
                T_min:units = "degC" ;
                T_min:long_name = "Interpolated temperature" ;
```

```
            T_min:statistic = "min" ;
    double T_max(feature_num) ;
            T_max:_FillValue = -9999. ;
            T_max:analysis_type = "values" ;
            T_max:units = "degC" ;
            T_max:long_name = "Interpolated temperature" ;
            T_max:statistic = "max" ;
    double RH_mean(feature_num) ;
            RH_mean:_FillValue = -9999. ;
            RH_mean:analysis_type = "values" ;
            RH_mean:units = "%" ;
            RH_mean:long_name = "Interpolated relative humidity" ;
            RH_mean:statistic = "mean" ;
    double RH_min(feature_num) ;
            RH_min:_FillValue = -9999. ;
            RH_min:analysis_type = "values" ;
            RH_min:units = "%" ;
            RH_min:long_name = "Interpolated relative humidity" ;
            RH_min:statistic = "min" ;
    double RH_max(feature_num) ;
            RH_max:_FillValue = -9999. ;
            RH_max:analysis_type = "values" ;
            RH_max:units = "%" ;
            RH_max:long_name = "Interpolated relative humidity" ;
            RH_max:statistic = "max" ;
    double p_mean(feature_num) ;
            p_mean:_FillValue = -9999. ;
            p_mean:analysis_type = "values" ;
            p_mean:units = "kPa" ;
            p_mean:long_name = "Interpolated air pressure" ;
            p_mean:statistic = "mean" ;
    double p_min(feature_num) ;
            p_min:_FillValue = -9999. ;
            p_min:analysis_type = "values" ;
            p_min:units = "kPa" ;
            p_min:long_name = "Interpolated air pressure" ;
            p_min:statistic = "min" ;
    double p_max(feature_num) ;
            p_max:_FillValue = -9999. ;
            p_max:analysis_type = "values" ;
            p_max:units = "kPa" ;
            p_max:long_name = "Interpolated air pressure" ;
            p_max:statistic = "max" ;
    double Fill_percent(feature_num) ;
            Fill_percent:_FillValue = -9999. ;
            Fill_percent:units = "%" ;
```

```
                Fill_percent:long_name = "Percentage of hydrometeor object\'s area excluding holes" ;
        double Solidity(feature_num) ;
                Solidity:_FillValue = -9999. ;
                Solidity:units = "1" ;
                Solidity:long_name = "Fraction of hydrometeor object\'s echoes relative to convex hull
area" ;
        double area(feature_num) ;
                area:_FillValue = -9999. ;
                area:units = "km^2" ;
                area:long_name = "area of hydrometeor field" ;
        double maximum_dimension(feature_num) ;
                maximum_dimension:_FillValue = -9999. ;
                maximum_dimension:units = "km" ;
                maximum_dimension:long_name = "Maximum dimension of hydrometeor field (using
maximum Feret diameter)" ;
        double ellipse_fit_centroid_x(feature_num) ;
                ellipse_fit_centroid_x:_FillValue = -9999. ;
                ellipse_fit_centroid_x:units = "m" ;
                ellipse_fit_centroid_x:long_name = "Fitted ellipse cetroid x (E/W) coordinate value" ;
        double ellipse_fit_centroid_y(feature_num) ;
                ellipse_fit_centroid_y:_FillValue = -9999. ;
                ellipse_fit_centroid_y:units = "m" ;
                ellipse_fit_centroid_y:long_name = "Fitted ellipse cetroid y (N/S) coordinate value" ;
        double ellipse_fit_orientation(feature_num) ;
                ellipse_fit_orientation:_FillValue = -9999. ;
                ellipse_fit_orientation:units = "degree" ;
                ellipse_fit_orientation:long_name = "Fitted ellipse orientation angle from the x (E/W)
plane counter-clockwise" ;
        double ellipse_fit_a_axis(feature_num) ;
                ellipse_fit_a_axis:_FillValue = -9999. ;
                ellipse_fit_a_axis:units = "km" ;
                ellipse_fit_a_axis:long_name = "Fitted ellipse semi-major axis length" ;
        double ellipse_fit_c_axis(feature_num) ;
                ellipse_fit_c_axis:_FillValue = -9999. ;
                ellipse_fit_c_axis:units = "km" ;
                ellipse_fit_c_axis:long_name = "Fitted ellipse semi-minor axis length" ;
        double x2_prom_peaks(feature_num) ;
                x2_prom_peaks:_FillValue = -9999. ;
                x2_prom_peaks:units = "1" ;
                x2_prom_peaks:long_name = "Number of peaks with prominenence of 2 times their
(linear scale) surrounding" ;
        double x5_prom_peaks(feature_num) ;
                x5_prom_peaks:_FillValue = -9999. ;
                x5_prom_peaks:units = "1" ;
                x5_prom_peaks:long_name = "Number of peaks with prominenence of 5 times their
(linear scale) surrounding" ;
```

```
double x10_prom_peaks(feature_num) ;
        x10_prom_peaks:_FillValue = -9999. ;
        x10_prom_peaks:units = "1" ;
        x10_prom_peaks:long_name = "Number of peaks with prominenence of 10 times their (linear scale) surrounding" ;
short second_trip_flag(feature_num) ;
        second_trip_flag:_FillValue = -9999s ;
        second_trip_flag:long_name = "1 - second trip suspect; 2 - (if not removed from dataset) second trip likely" ;
        second_trip_flag:units = "1" ;
int sweep(feature_num) ;
        sweep:_FillValue = -9999 ;
        sweep:long_name = "Sweep number" ;
        sweep:units = "1" ;
float mean_elevation_angle(feature_num) ;
        mean_elevation_angle:_FillValue = -9999.f ;
        mean_elevation_angle:long_name = "Mean elevation angle in sweep" ;
        mean_elevation_angle:units = "degree" ;
int feature_num(feature_num) ;
        feature_num:long_name = "Feature number" ;
        feature_num:units = "1" ;
double feature_time(feature_num) ;
        feature_time:_FillValue = -9999. ;
        feature_time:long_name = "Radar sweep time per feature" ;
        feature_time:units = "seconds since 2020-03-13 00:01:29 0:00" ;
double time(time) ;
        time:long_name = "Time in seconds since volume start" ;
        time:units = "seconds since 2020-03-13 00:01:29 0:00" ;
double time_offset(time) ;
        time_offset:_FillValue = -9999. ;
        time_offset:long_name = "Time offset from base_time" ;
        time_offset:units = "seconds since 2020-03-13 00:01:29 0:00" ;
int base_time ;
        base_time:_FillValue = -9999 ;
        base_time:long_name = "Base time in Epoch" ;
        base_time:units = "seconds since 1970-01-01 0:00:00 0:00" ;
double lat ;
        lat:_FillValue = -9999. ;
        lat:long_name = "North latitude" ;
        lat:units = "degree_N" ;
double lon ;
        lon:_FillValue = -9999. ;
        lon:long_name = "longitude" ;
        lon:units = "degree_E" ;
double alt ;
        alt:_FillValue = -9999. ;
```

```
		alt:long_name = "Altitude above mean sea level" ;
		alt:units = "m" ;

// global attributes:
		:location_description = "Cold-Air Outbreaks in the Marine Boundary Layer Experiment (COMBLE), Andoy, Norway" ;
		:doi = "10.5439/2203039" ;
		:dod_version = "v1.0" ;
		:command_line = "python SACR_cluster_main.py" ;
		:datastream = "anxkasacrppihydfeatM1.c1" ;
		:data_level = "c1" ;
		:facility_id = "M1" ;
		:site_id = "anx" ;
		:platform_id = "kasacrppihydfeat" ;
		:history = "created by user isilber1 on machine dev-proc2 at 12-Apr-2024,23:00:40" ;
```

Appendix B

Feature Mask Output Data

```
netcdf anxkasacrppihydmaskM1.c1.20200313.000000 {
dimensions:
	time = UNLIMITED ; // (238 currently)
	y = 1601 ;
	x = 1601 ;
	string43 = 43 ;
variables:
	double time(time) ;
		time:long_name = "Time in seconds since volume start" ;
		time:units = "seconds since 2020-03-13 00:01:29 0:00" ;
	double y(y) ;
		y:standard_name = "projection_y_coordinate" ;
		y:long_name = "Y distance on the projection plane from the origin" ;
		y:units = "m" ;
	double x(x) ;
		x:standard_name = "projection_x_coordinate" ;
		x:long_name = "X distance on the projection plane from the origin" ;
		x:units = "m" ;
	int segmentation_mask(time, y, x) ;
		segmentation_mask:_FillValue = -9999 ;
		segmentation_mask:long_name = "segmentation_mask" ;
		segmentation_mask:units = "1" ;
	double corresponding_angle(time) ;
		corresponding_angle:_FillValue = -9999. ;
		corresponding_angle:long_name = "Mean elevation angle corresponding to time step" ;
		corresponding_angle:units = "degree" ;
	double corresponding_sweep(time) ;
		corresponding_sweep:_FillValue = -9999. ;
		corresponding_sweep:long_name = "Sweep corresponding to time step" ;
		corresponding_sweep:units = "1" ;
	char corresponding_files(time, string43) ;
		corresponding_files:long_name = "File name corresponding to time step" ;
		corresponding_files:units = "1" ;
		corresponding_files:_Encoding = "utf-8" ;
```

```
	double corresponding_t_step(time) ;
		corresponding_t_step:_FillValue = -9999. ;
		corresponding_t_step:long_name = "Time step (frame) corresponding to segments time
step" ;
		corresponding_t_step:units = "1" ;
	double time_offset(time) ;
		time_offset:_FillValue = -9999. ;
		time_offset:long_name = "Time offset from base_time" ;
		time_offset:units = "seconds since 2020-03-13 00:01:29 0:00" ;
	int base_time ;
		base_time:_FillValue = -9999 ;
		base_time:long_name = "Base time in Epoch" ;
		base_time:units = "seconds since 1970-01-01 0:00:00 0:00" ;
	double lat ;
		lat:_FillValue = -9999. ;
		lat:long_name = "North latitude" ;
		lat:units = "degree_N" ;
	double lon ;
		lon:_FillValue = -9999. ;
		lon:long_name = "longitude" ;
		lon:units = "degree_E" ;
	double alt ;
		alt:_FillValue = -9999. ;
		alt:long_name = "Altitude above mean sea level" ;
		alt:units = "m" ;

// global attributes:
		:num_sweeps = "3" ;
		:edge_indices_for_sweep_1 = "[24, 1576]" ;
		:edge_indices_for_sweep_2 = "[24, 1575]" ;
		:edge_indices_for_sweep_3 = "[25, 1575]" ;
		:location_description = "Cold-Air Outbreaks in the Marine Boundary Layer Experiment
(COMBLE), Andoy, Norway" ;
		:doi = "10.5439/2203040" ;
		:dod_version = "v1.0" ;
		:command_line = "python SACR_cluster_main.py" ;
		:datastream = "anxkasacrppihydmaskM1.c1" ;
		:data_level = "c1" ;
		:facility_id = "M1" ;
		:site_id = "anx" ;
		:platform_id = "kasacrppihydmask" ;
		:history = "created by user isilber1 on machine dev-proc2 at 12-Apr-2024,23:00:40" ;
}}
```

www.arm.gov

U.S. DEPARTMENT OF
ENERGY

Office of Science